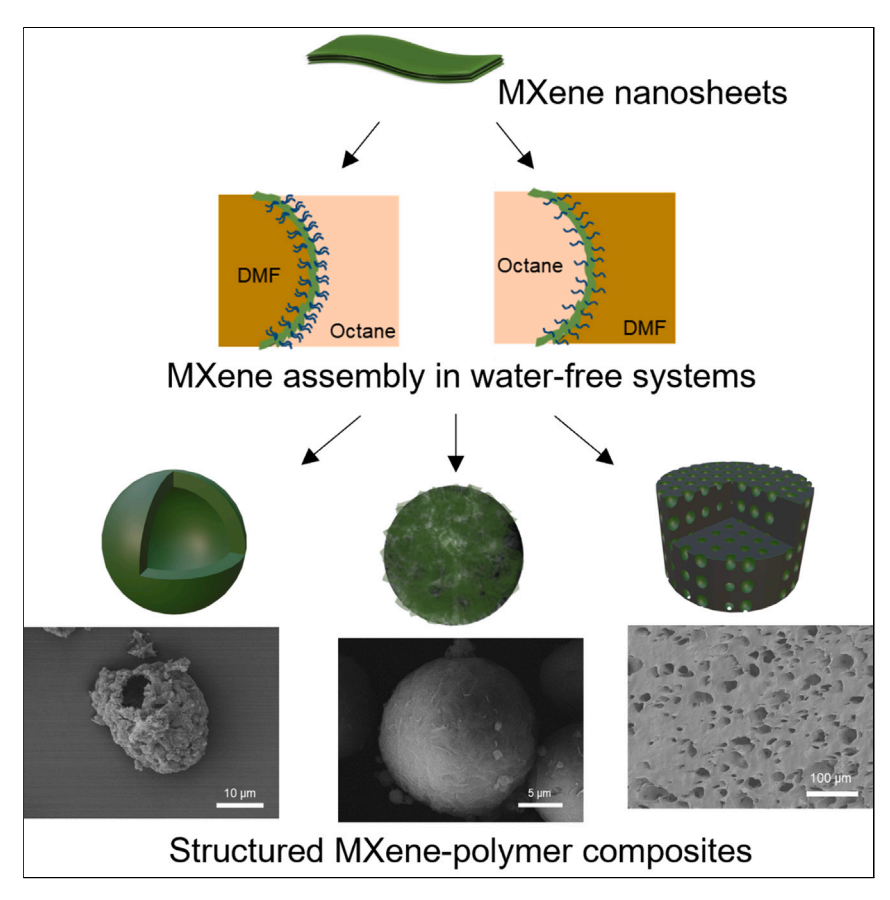
Matter



Article

Structured Ti₃C₂T_z MXene-polymer composites from non-aqueous emulsions



This work demonstrates a straightforward method to fabricate structured MXene-polymer composites with controlled filler distribution and composite morphology in a water-free system by emulsion-assisted polymerization. Either the droplets, interfaces, or continuous phase can be polymerized to form particles, capsules, or foams, respectively. These non-aqueous systems provide opportunities for new compositions, including those that are sensitive to water.

Huaixuan Cao, Yifei Wang, Zeyi Tan, ..., Miladin Radovic, Emily B. Pentzer, Micah J. Green

emilypentzer@tamu.edu (E.B.P.) micah.green@tamu.edu (M.J.G.)

Highlights

Controllable non-aqueous emulsions were developed using modified MXenes

Structured MXene-polymer composites were fabricated by emulsion polymerization

Either the droplets, interfaces, or continuous phase can be polymerized

Rapid RF heating was demonstrated on structured MXene-polymer composites



Matter



Article

Structured Ti₃C₂T_z MXene-polymer composites from non-aqueous emulsions

Huaixuan Cao,¹ Yifei Wang,² Zeyi Tan,² Ethan Harkin,¹ Smita Shivraj Dasari,¹ Jodie L. Lutkenhaus,^{1,2} Miladin Radovic,² Emily B. Pentzer,^{2,3,*} and Micah J. Green^{1,2,4,*}

SUMMARY

To date, major challenges in constructing MXene-polymer composites include incompatible processing conditions and poor control over the organization of MXenes within the polymer matrix. Here, we report a new approach to create MXene-polymer composites in a water-free system by alkylating the nanosheets via electrostatic adsorption of alkyl ammoniums and then using them as surfactants in oil-in-oil emulsions, followed by polymerization. Within these MXene-stabilized non-aqueous emulsions, polymerization of continuous phase, discontinuous phase, and interface result in composite foams, armored particles, and capsules, respectively. This nonaqueous system significantly expands MXene-polymer architecture compositions and highlights the ability to control both nanosheet distribution and composite morphology. We also showcase the rapid volumetric heating of the distinct MXene foam structure in response to low-power radiofrequency fields. This work highlights the importance and opportunities of disconnecting composition and structure to advance fundamental understandings and access new performance-related properties.

INTRODUCTION

The ability to control the placement and/or orientation of particles within a polymer can lead to enhanced performance-related properties, in complement to controlling composition of the composite. In much of the composite literature, focus is placed on preventing particle aggregation, dispersing particle fillers throughout the polymer matrix, or creating a percolated network of particles through the matrix. Common fabrication methods for polymer composites, such as solution mixing, melt processing, and in situ polymerization, typically lead to composites in which particulate filler is dispersed homogeneously throughout the polymer matrix. 1-5 However, by controlling the microscopic and macroscopic structures of composites, substantial enhancement of material properties may be possible. ^{6–10} For instance, Ma et al. reported high electromagnetic interference (EMI) shielding properties of a segregated Ti₃C₂T_z-polypropylene composite film that was prepared by microwave sintering of Ti₃C₂T_z-coated polypropylene particles. Another example of structured polymer composite was reported by Wang et al., who developed a gradient-layered barium titanate/poly(vinylidene fluoride) composite with a high energy density and chargedischarge efficiency using a layer-by-layer casting method. 10

Of the various approaches to preparing structured composites, including layer-by-layer assembly, ^{11–13} template coating, ^{14–17} and polymer impregnation, ^{18–20} Pickering emulsion templating is attractive due to the well-defined interfaces, controllable

PROGRESS AND POTENTIAL

MXene-polymer composites have gained great attention due to their favorable electrical properties and applications across electromagnetic interference (EMI) shielding, energy storage, gas separation, water purification, and catalysis. The traditional way to fabricate MXene-polymer composites involves direct mixing of MXene and polymer in a solution or melt, leading to a homogeneous structure, which has limited control over filler distribution and has incompatibility issues with hydrophobic polymers. This report develops a simple and generalized approach to create structured MXene-polymer composites in a water-free system with well-controlled filler distribution and varied composite morphology (e.g., capsules, armored particles, and porous foams). This research not only expands the possible compositions of MXene-polymer architectures but also provides insights into their structureproperty relationships, paving the way for developing desired performance-related properties.





structure and size of droplets, and ease of scale-up. 21-24 In Pickering emulsions, solid particle surfactants stabilize a mixture of two immiscible liquids (e.g., oil and water), with droplets of one being dispersed in a continuous phase of the other. Localization of monomers within Pickering emulsions can lead to the formation of composite shells, armored polymer particles, or porous polymer monoliths coated with surfactant particles. 25-28 For example, polymerization of the droplets (i.e., dispersion polymerization) yields solid polymer spheres coated with nanoparticle surfactants, whereas polymerization of the continuous phase results in a foam with pores coated with the nanoparticle surfactants. Lastly, polymerization between one monomer in the discontinuous phase and the other in the continuous phase, e.g., at the emulsion interface, gives capsule shells of polymer with Pickering nanoparticles embedded within. Pickering emulsions are also valuable in that the particles can serve a dual purpose: stabilizing the emulsion and imparting functional properties in the composite produced. These functional properties are often connected with the electrical or thermal conductivity of the particles themselves.^{29–32} For example, Yu et al. reported the fabrication of conductive cellulose nanocrystals/carbon nanotubes/polylactide films with high EMI-shielding performance using the Pickering emulsion template method, where the carbon nanotubes serve as both particle surfactants and conductive network.31

Two-dimensional (2D) particles are of great interest as Pickering surfactants, including the relatively new class of 2D nanoparticles MXenes, or transition metal carbides, nitrides, or carbonitrides. Compared to spherical particles, nanosheets have large surface area and high aspect ratio to cover more liquid-liquid interfaces, and, compared to small-molecule surfactants, it takes substantially more energy to remove particles from the interface. Common 2D surfactants that have been coupled with polymerizations include clay platelets,³³ layered double hydroxides, 34,35 and graphene oxide (GO) nanosheets. 36,37 For example, our group reported Pickering emulsions stabilized GO to prepare hollow capsules, ionicliquid-filled capsules, and armored polymer particles.^{38–41} Similarly, Xie et al. fabricated wrinkled spherical GO/polystyrene particles from Pickering emulsions, 42 and Yang et al. synthesized GO-based porous conductive foams with enhanced piezoresistive properties from high-internal-phase emulsions (HIPEs).⁴³ In complement to these more common 2D particle surfactants, MXenes are attractive as they not only can stabilize emulsions but also hold the potential to impart functional properties into structures. MXenes have a general formula of $M_{n+1}X_nT_z$, where M is transition metal (e.g., Ti, V, Nb), X is carbon and/or nitrogen, and Tz is a general term for surface terminal groups (e.g., -OH, -F, -Cl, -Br). 44-47 Not only are MXenes processable as aqueous solutions but they also have distinct properties, including high electrical conductivity, ⁴⁸⁻⁵⁰ high catalytic properties, ⁵¹⁻⁵³ and versatile compositions, 54,55 rendering them exciting fillers in polymers. The interfacial assembly of MXenes in water-based Pickering emulsions provides a simple way to fabricate structured MXene composites.⁵⁶⁻⁶² For example, our group demonstrated that Ti₃C₂T₇ nanosheets can stabilize oil-in-water Pickering emulsions provided an aqueous dispersion of nanosheets is flocculated with salt.⁶³ Polystyrene particles armored with Ti₃C₂T_z nanosheets prepared by dispersion polymerization were used as feedstock to prepare films with the nanosheets organized into a honeycomb network; these structures had application in EMI shielding and radiofrequency (RF) heating.⁶⁴ In complement, Zheng et al. prepared conductive porous foams of $Ti_3C_2T_z$ and crosslinked polystyrene via polymerization of continuous phase of water-in-oil HIPEs,⁶¹ and Fan et al. fabricated Ti₃C₂T_z-containing porous structures by polymerizing a mixture of ionic and neutral monomers (i.e., 3-dodecyl-1-vinylimidazolium bromide, 3-hexadecyl-1-vinylimidazolium bromide,

https://doi.org/10.1016/j.matt.2024.02.011

¹Artie McFerrin Department of Chemical Engineering, Texas A&M University, College Station, TX LICA

²Department of Materials Science and Engineering, Texas A&M University, College Station, TX, USA

³Department of Chemistry, Texas A&M University, College Station, TX, USA

⁴Lead contact

^{*}Correspondence: emilypentzer@tamu.edu (E.B.P.), micah.green@tamu.edu (M.J.G.)



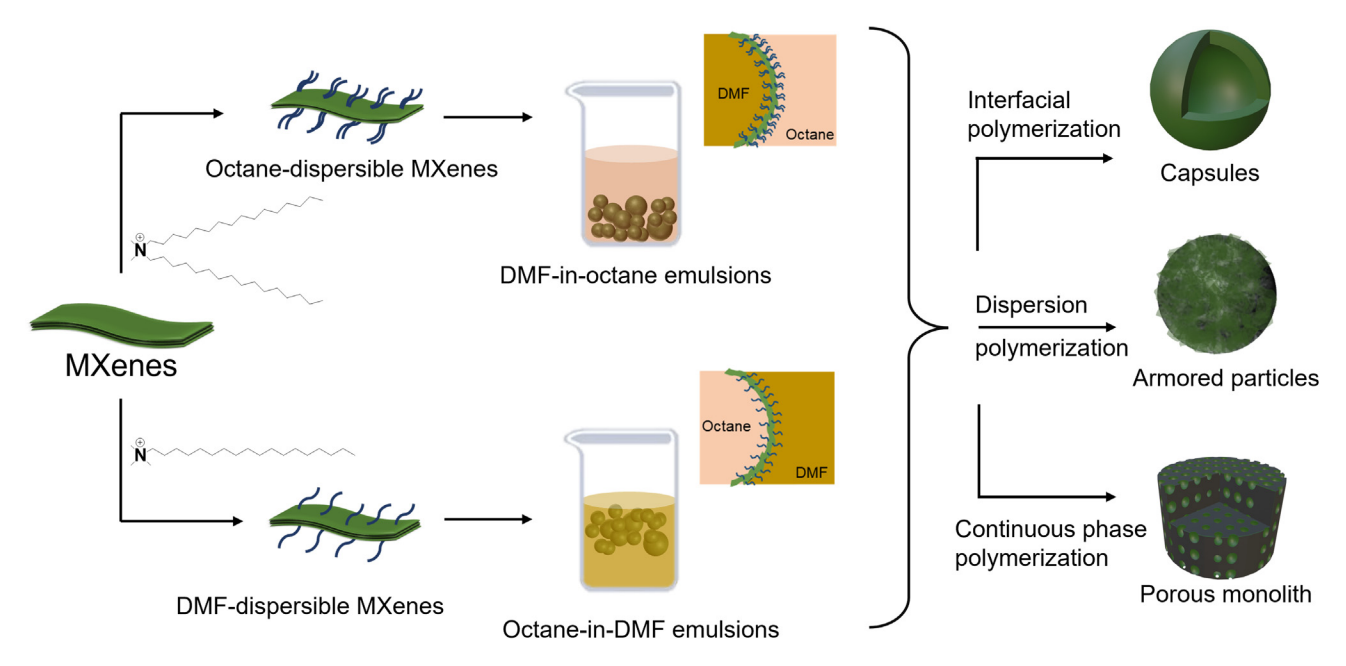
and methyl methacrylate) in water-in-ionic-liquid HIPEs for use as piezoresistive sensor and oil/water separation applications.⁶²

The production of structured MXene-polymer composites from emulsions has, to date, been limited to water-based systems; the ability to expand the types of interfaces (e.g., oil-oil, oil-ionic-liquid, etc.) holds the potential to dramatically enhance the accessible structures and compositions that can be used to define structurefunction relationships and enhance performance-related properties in, for example, encapsulation, catalysis, and thermal energy management. 65-68 In these emulsions. the two phases must be immiscible and commonly one is polar (e.g., N,N-dimethylformamide [DMF] or ionic liquid) and the other is nonpolar (e.g., hydrocarbon). Traditional surfactants for stabilizing these oil-oil emulsion are block copolymers with the relative block length and polymer identity specific to the oils selected. 69-71 For example, Müller et al. reported the synthesis of high-molecular-weight polyurethane particles using polyaddition of diisocyanates (4,4'-methylenebis(cyclohexyl isocyanate)) and diols (ethylene glycol and 1,4-bis(hydroxymethyl)cyclohexane) in DMF-in-hexane emulsions stabilized by poly(isoprene)-poly(methyl methacrylate) block copolymer.⁷² Nanoparticles, such as modified silica^{73,74} and alkylated cellulose, 67 have been sued to stabilize oil-oil Pickering emulsions. Our group demonstrated that alkylation of GO gives 2D particles that can stabilize oil-in-oil and other non-aqueous emulsions, enabling the production of composites with water-sensitive components. 75-79 For example, Rodier et al. reported the formation of polyisocyanoethyl methacrylate particles with intact isocyanate groups from C₁₈-GO stabilized DMF-in-dodecane emulsions.⁷⁸ Similarly, Wang et al. utilized C₁₈-GO to stabilize DMF-in-octane emulsions for the synthesis of temperature-dependent hindered poly(urea-urethane) capsules.⁷⁹ Further, Lak et al. used alkylated nanosheets to encapsulate magnesium nitrate hexahydrate (MNH) by precipitation of polymers in molten MNH-in-toluene emulsions and used these structures for thermal energy management.⁷⁵ Unlike other 2D particle surfactants, MXenes hold the potential to impart functional properties without significant post-processing (e.g., chemical reduction of GO), and MXenes must be developed as particle surfactants in oil-oil systems for the formation of structured polymer composites.

Here, for the first time, we report the functionalization of Ti₃C₂T₂ MXenes for stabilization of both polar-in-nonpolar and nonpolar-in-polar non-aqueous Pickering emulsions and the use of these emulsions for the synthesis of structured capsules, particles, and porous monolith. As is indicated in Scheme 1 (top), DMF-in-octane emulsions are stabilized by Ti₃C₂T_z nanosheets modified by dihexadecyl dimethylammonium bromide (DHDAB), whereas octane-in-DMF emulsions (Scheme 1, bottom), are stabilized by Ti₃C₂T₂ modified with octadecyl trimethylammonium bromide (OTAB). This difference in nanosheet functionalization with a single or double long alkyl chain controls the hydrophobicity to the nanosheets, and thus their dispersibility, with the solvent serving as the continuous phase of the emulsion they stabilize (i.e., Bancroft rule). As a result, we can create controllable MXene oil-oil emulsions (polar in nonpolar or nonpolar in polar) for selective emulsion polymerizations (such as in the dispersed phase, the continuous phase, or at the interface). Specifically, we leverage three polymerization approaches in these Pickering emulsions to prepare composite structures: polymerization of the interface to give composite capsules shells, polymerization of the dispersed phase to give polymer particles armored with nanosheets, and polymerization of the continuous phase to fabricate porous monoliths coated with nanosheets. To demonstrate the unique properties of our structured MXene-polymer composites, we measured the RF heating response of the MXene porous monolith, and it exhibits rapid and







Scheme 1. Overview of the approach to prepare MXene-stabilized oil-in-oil emulsions and their use in fabrication of structured materials Top approach shows the functionalization of $Ti_3C_2T_z$ with a double long-alkyl-chain ammonium salt (DHDAB) for polar-in-nonpolar emulsions; bottom approach shows the functionalization of $Ti_3C_2T_z$ with a single long-alkyl-chain ammonium salt (OTAB) for nonpolar-in-polar emulsions.

steady heating from room temperature to $54^{\circ}C$ in response to RF field at low power of 1 W and this RF heating performance is distinctly higher than that of the homogeneous MXene/polymer counterparts reported in our prior work ($Ti_3C_2T_z/polyvinyl$ alcohol composites with nearly no heating response with similar low loading of $Ti_3C_2T_z$ at 1 W), 80 indicating the formation of conductive MXene network in the structured polymer composites. These results demonstrate a straightforward and generalized approach for the fabrication of structured MXene-polymer composites from non-aqueous system, giving access to new MXene-polymer architecture with tailorable compositions that use composition and structure to enable performance-related properties.

RESULTS AND DISCUSSION

Preparation and characterization of Ti₃C₂T_z MXenes

To demonstrate that surface functionalization can be used to modify MXenes and enable their use as particle surfactants to stabilize non-aqueous emulsions, Ti₃C₂T_z nanosheets were prepared and characterized as previously reported.⁸¹ To prepare the nanosheets, the Al layer in Ti₃AlC₂ MAX powder was selectively etched with an aqueous LiF/HCl solution and then the resulting $Ti_3C_2T_z$ clay (multi-layer) was isolated and subjected to intercalation with DMSO and exfoliation to yield $Ti_3C_2T_z$ nanosheets. The aqueous suspension of Ti₃C₂T_z nanosheets was a dark green color with a ~ -40 mV ζ potential, indicating good colloidal stability in water. Figure S1A shows the X-ray diffraction (XRD) curve of an as-prepared free-standing Ti₃C₂T₇ nanosheet film prepared by vacuum-assisted filtration with the characteristic 002 peak observed at 5.4°, indicating the successful etching and exfoliation of the nanosheets. Figure S1B shows the scanning electron microscopy (SEM) images of freezedried $Ti_3C_2T_z$ nanosheets and Figure S1C shows the transmission electron microscopy (TEM) images of the drop-cast nanosheets on a hollow carbon grid, indicating successful exfoliation of single- or few-layer nanosheets with the lateral size of hundreds of nanometers to a few micrometers.



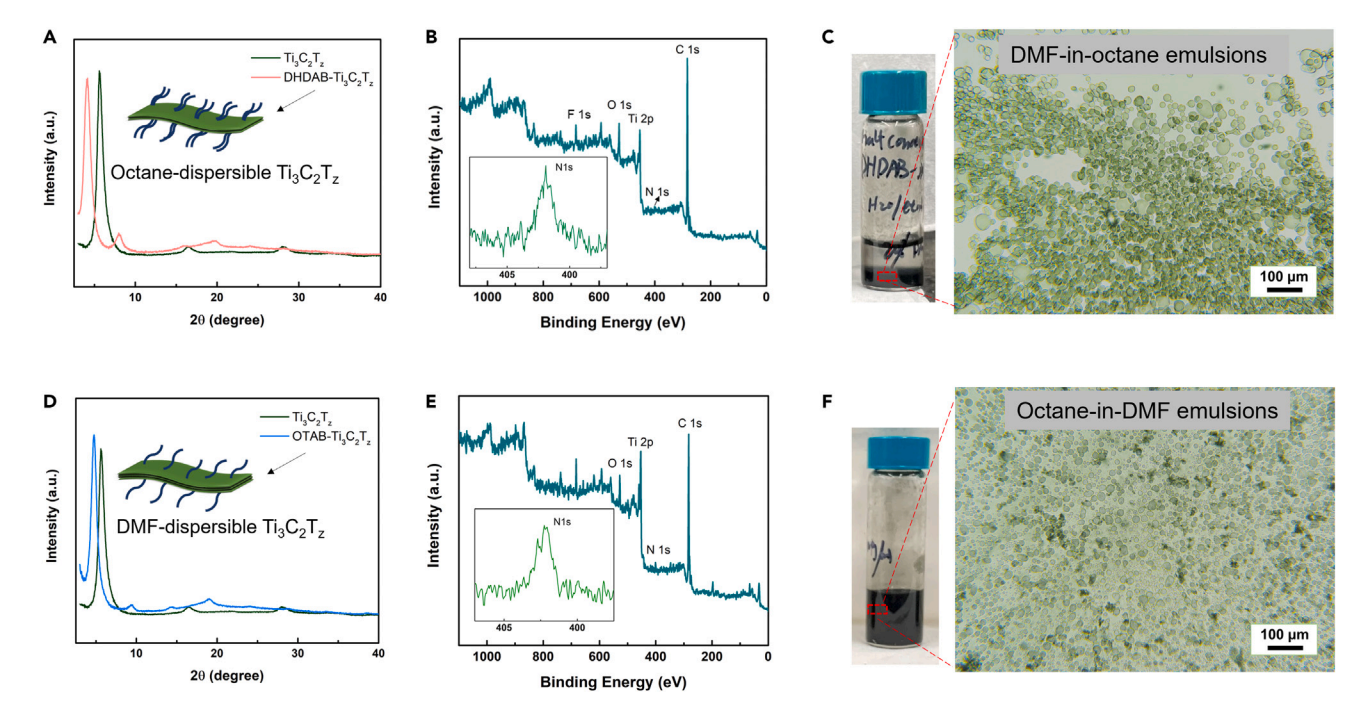


Figure 1. Characterization of DHDAB-modified Ti₃C₂T_z and their use in stabilizing oil-oil Pickering emulsions

- (A) XRD of pure $Ti_3C_2T_z$ nanosheets and DHDAB- $Ti_3C_2T_z$.
- (B) XPS survey spectrum of DHDAB- $Ti_3C_2T_z$ (inset is high-resolution N 1s peak).
- (C) Vial and optical microscopy image of DMF-in-octane emulsions stabilized by DHDAB-Ti $_3$ C $_2$ T $_z$ (1 mg/mL DHDAB-Ti $_3$ C $_2$ T $_z$, 1:5 v/v of DMF:octane). Scale bar: 100 μ m.
- (D) XRD of pure $Ti_3C_2T_z$ nanosheets and OTAB- $Ti_3C_2T_z$.
- (E) XPS survey spectrum of OTAB-Ti $_3$ C $_2$ T $_z$ (inset is the high-resolution N 1s peak).
- (F) Vial and optical microscopy image of octane-in-DMF emulsions stabilized by OTAB-Ti $_3$ C $_2$ T $_z$ (1 mg/mL OTAB-Ti $_3$ C $_2$ T $_z$, 1:5 v/v of octane:DMF). Scale bar: 100 μ m.

Ti₃C₂T_z MXene functionalization and Pickering emulsions

In order to stabilize non-aqueous emulsions, the Ti₃C₂T₇ nanosheets were modified with organic small molecules via electrostatic interactions. To stabilize polar-innonpolar oil-oil emulsions, the Ti₃C₂T_z nanosheets were modified with a double long-alkyl-chain ammonium salt (DHDAB), which transformed the water-dispersible nanosheets to octane-dispersible nanosheets. In this system, the cationic ammonium head group interacts electrostatically with the negatively charged faces of the nanosheets, effectively hydrophobizing the nanosheets. To complete this functionalization, a dispersion of Ti₃C₂T_z nanosheets in a mixture of water and ethanol was added to a solution of DHDAB in the same solvent mixture (mass ratio of $Ti_3C_2T_z$ to DHDAB = 1:1). The nanosheets precipitated from solution and were isolated by centrifugation then washed to remove excess DHDAB. Then the nanosheets were suspended in octane to make a DHDAB-Ti₃C₂T₂ octane dispersion, which was stable to standing for 48 h (Figures S2A and S2B). Note that as-prepared Ti₃C₂T₇ nanosheets were not stable as an octane dispersion and rapidly precipitated. The stability of the modified nanosheet dispersion in octane can be attributed to the increased hydrophobicity upon modification with DHDAB, supported by water contact angle measurements of pure Ti₃C₂T_z buckypaper and DHDAB-Ti₃C₂T_z buckypaper of 57.2° and 128.0°, respectively (Figures S1D and S2C). SEM imaging of freezedried DHDAB-Ti₃C₂T_z demonstrates the nanosheet structure is maintained upon functionalization (Figure S2D). In XRD spectra, the characteristic 002 peak of as-prepared Ti₃C₂T_z (5.4°) shifts to 4.1° upon DHDAB functionalization (Figure 1A),





indicating increased interlayer spacing upon modification due to long alkyl chains of DHDAB. To further confirm functionalization with DHDAB, X-ray photoelectron spectroscopy (XPS) was employed. In the XPS survey spectrum of DHDAB-Ti₃C₂T_z, the elements Ti, C, O, and F are identified (Figure 1B), and the high-resolution N 1s peak confirms the presence of DHDAB functionalization (Figure 1B, inset). In addition, the Fourier transform infrared (FTIR) spectroscopy of the DHDAB-Ti₃C₂T₇ (Figure S3) shows distinct C-H stretching peaks around 2,848 cm⁻¹ and 2,914 cm⁻¹ compared to pristine $Ti_3C_2T_z$ (no significant peak at \sim 2,800–2,900 cm⁻¹), indicating the successfully functionalization of long alkyl chains from DHDAB. To probe the thermal stability of the modified $Ti_3C_2T_z$, thermogravimetric analysis (TGA) was done on the pristine Ti₃C₂T₇ (Figure S4A) and DHDAB-Ti₃C₂T₇ (Figure S4B). No obvious mass change was observed for the pristine Ti₃C₂T_z, indicating the good thermal stability of $Ti_3C_2T_z$ nanosheets up to 700°C. For the DHDAB- $Ti_3C_2T_z$, the degradation of DHDAB is observed from $\sim 250^{\circ}$ C to 400° C and around 74.6 wt % remains after heating up to 700°C, which can be attributed to the Ti₃C₂T_z nanosheets. This suggests the DHDAB functionalization on the $Ti_3C_2T_z$ nanosheets starts to leave and degrade at around 250°C.

The successful functionalization of DHDAB-Ti₃C₂T_z and dispersibility in octane enable their use to stabilize DMF-in-octane Pickering emulsions. To form an emulsion, DMF was added to an octane dispersion of DHDAB-Ti₃C₂T_z (1 mg/mL) then subjected to high-shear mixing. This resulted in a milky solution consisting of droplets of DMF dispersed in octane, with the nanosheets located at the oil-oil interface, and, upon standing, a dense layer of emulsion formed at the bottom of the vial (Figure 1C). The as-prepared DMF-in-octane emulsion droplets were characterized by optical microscopy, which showed uniform and neat emulsion droplets (average size $\sim\!15~\mu m$; Figure S5A) with good spheric shape and dark green contrast (Figure 1C), supporting that the nanosheets were associated with the interface. Leaving the emulsions unagitated over a course of 1 month did not lead to an appreciable change in the droplets, which indicates good emulsion stability and that this system can be used to prepare structured polymer composites (Figures S6A–S6D).

The ability to control the polarity of the continuous and discontinuous phase gives further control of composite composition and we thus sought to modify the nanosheets so they could stabilize the inverse nonpolar-in-polar emulsions (e.g., octane-in-DMF) (Scheme 1, bottom). To do so, a single long-alkyl-chain ammonium salt (OTAB) was used to functionalize Ti₃C₂T_z nanosheets in a similar method as described above (mass ratio of $Ti_3C_2T_z$ to OTAB = 1:1). A DMF dispersion of OTAB-Ti₃C₂T_z was stable for 48 h (Figures S7A and S7B), and the water contact angle of OTAB-Ti₃C₂T_z nanosheets had intermediate wettability to as-prepared Ti₃C₂T_z and DHDAB-Ti₃C₂T_z (94.2° versus 57.2° and 128.0°; Figure S7C). The morphology of freeze-dried OTAB-Ti₃C₂T_z was characterized by SEM, which supports that the nanosheet structure was maintained after functionalization (Figure S7D). The XRD spectrum of OTAB-Ti₃C₂T₂ shows the characteristic 002 peak of the nanosheets at 4.8° , which is shifted 0.6° from that of as-prepared $Ti_3C_2T_z$ (5.4° ; Figure 1D). As with DHDAB-Ti₃C₂T_z, this shift is due to the increased interlayer spacing due to incorporation of OTAB molecules on the surface of the $Ti_3C_2T_z$ nanosheets. To confirm the composition of OTAB-Ti₃C₂T_z, XPS survey spectrum was used; Figure 1E shows the survey XPS spectrum and the presence of C, O, Ti, N, and F, all characteristic elements of Ti₃C₂T_z and OTAB (the high-resolution N 1s peak is shown in the inset). The successfully functionalization is also verified from the FTIR results by the C-H stretching (2,850 cm⁻¹ and 2,923 cm⁻¹) of OTAB-Ti₃C₂T_z nanosheets (Figure S3). The thermal stability of the OTAB-Ti₃C₂T_z nanosheets is characterized by





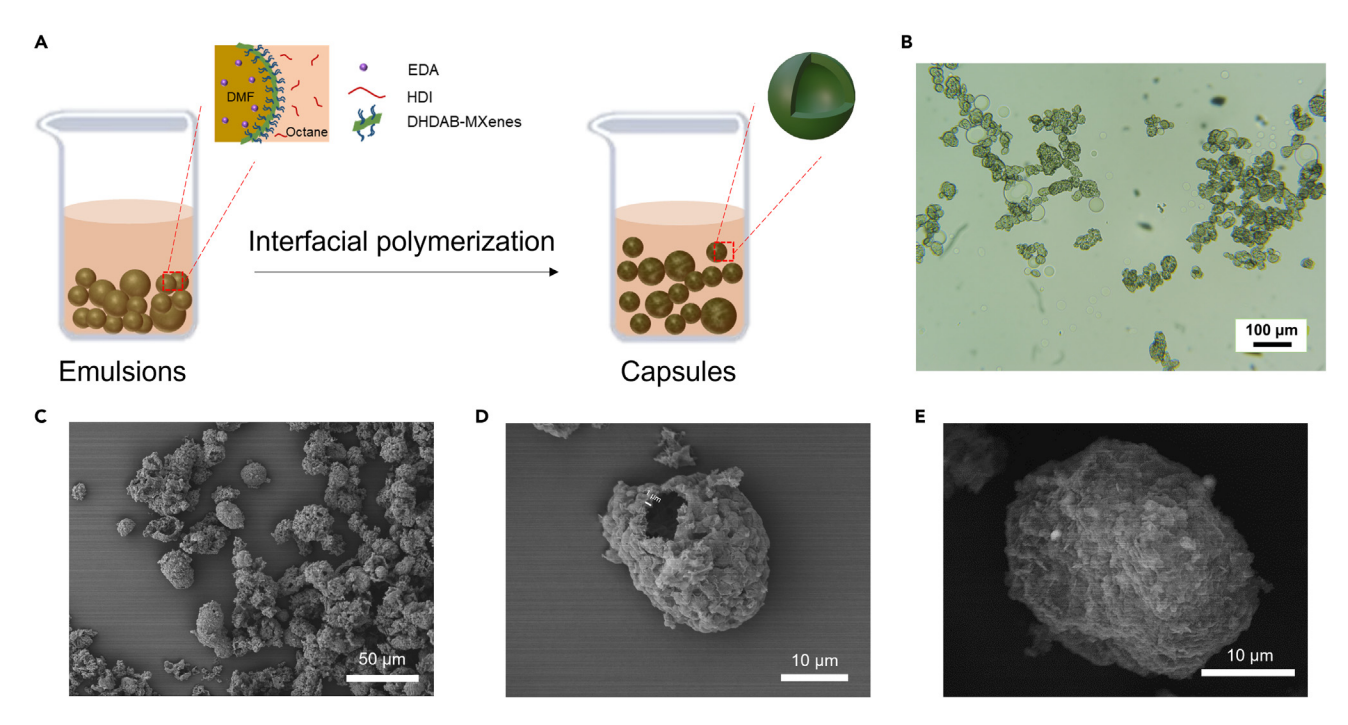


Figure 2. Composite capsule shells from DMF-in-octane emulsions using DHDAB-Ti₃C₂T_z (1 mg/mL, 1:5 v/v of DMF:octane) (A) Synthetic scheme.

(B) Optical microscopy image. Scale bar: $100 \mu m$.

(C–E) SEM images at different magnifications. Scale bars: 50 μm (C), 10 μm (D and E).

TGA (Figure S4C) and the OTAB degrades from $\sim 200^{\circ}\text{C}$ to 350°C , with around 76.0 wt % remaining mass at 700°C . OTAB- $\text{Ti}_3\text{C}_2\text{T}_z$ nanosheets are dispersible in DMF and, upon addition of octane and shear mixing, form stable octane-in-DMF emulsions with spherical droplets (average size, $\sim 14~\mu\text{m}$; Figure S5B), as observed with optical microscopy (Figure 1F). These octane-in-DMF emulsion droplets are still present after standing for 48 h (Figure S8), allowing for emulsion polymerization and fabrication of structured polymer composites. As we now had access to both nonpolar-in-polar and polar-nonpolar Pickering emulsions, we set out to utilize these platforms for compartmentalization of reagents and polymerizations to prepare structured MXene-polymer composites.

Synthesis of capsules from DMF-in-octane emulsions

To prepare ${\rm Ti_3C_2T_2}$ -polymer composite capsule shells, interfacial polymerization of two monomers in a non-aqueous emulsion was used. Here, an octane dispersion of DHDAB- ${\rm Ti_3C_2T_z}$ was used, a DMF solution of ethylenediamine (EDA) added, it was agitated to form DMF-in-octane Pickering emulsions, and then hexamethylene dissocyanate (HDI) was added to the continuous octane phase, as outlined in Figure 2A. Upon standing, interfacial step growth polymerization between the diisocyanate and the diamine produced a polyurea shell around the nanosheets surrounding the droplets. After 72 h, characterization of the samples using optical microscopy shows rough, semispherical capsules (Figure 2B), indicating successful formation of polyurea shell around the droplets. The isolated and dried capsules were characterized using SEM, which again supports semispherical structures with a thin hollow shell (Figures 2C–2E), confirming interfacial polymerization.

To confirm the composition of the capsule shells and the presence of both $Ti_3C_2T_z$ and polyurea, energy-dispersive X-ray spectroscopy (EDS) and XPS were used. As



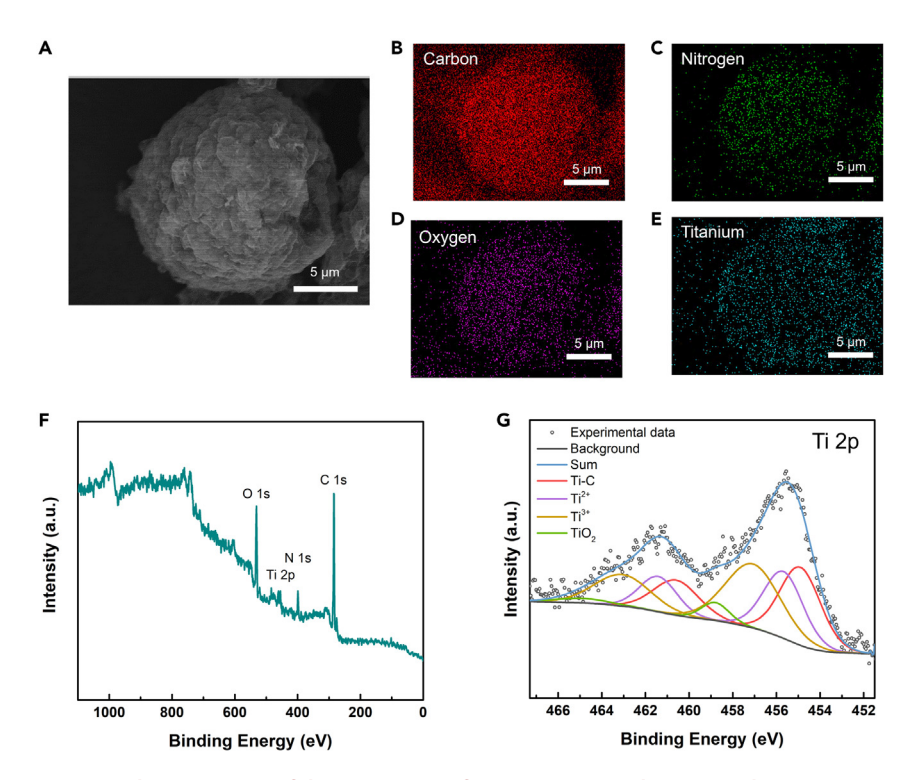


Figure 3. Characterization of the composition of DHDAB- $T_{i_3}C_2T_z$ -polyurea capsules (A) SEM image. Scale bar: 5 μ m. (B–E) EDS mapping (C, N, O, and Ti) corresponding to the SEM image in (A). Scale bars: 5 μ m. (F) XPS survey spectrum.

(G) Deconvoluted XPS high-resolution Ti 2p peak.

is shown in Figures 3A-3E, the EDS mapping of the DHDAB-Ti₃C₂T₂-polyurea capsules shows the uniform distribution of C, N, O, and Ti elements over the spheric shape, indicating the distribution of nanosheets within the polyurea shell. The survey XPS spectrum (Figure 3F) further confirms the presence of C, N, O, and Ti (72.6 atom %, 7.01 atom % 18.01 atom %, and 2.38 atom %, respectively; Table S1) near the capsule surface. Deconvolution of high-resolution of C 1s (Figure S9A) and O 1s (Figure S9B) shows the characteristic C-N and N-C=O peaks, indicating the presence of polyurea. Deconvolution of the high-resolution Ti 2p peak shows the characteristic Ti chemical bonding (Ti–C, Ti^{2+} , Ti^{3+} , TiO_2) in $Ti_3C_2T_z$ nanosheets (Figure 3G). Notably, the TiO₂ peak at 458.8 eV (green curve) contributes to only 5.1% of the Ti 2p signal, indicating that no significant oxidation of the nanosheet occurs during emulsification, interfacial polymerization, and isolation. Thus, both EDS and XPS support the Ti₃C₂T_z composition within the polyurea. Notably, the DHDAB- $Ti_3C_2T_z$ -polyurea capsules had less oxidation of $Ti_3C_2T_z$ compared to capsules obtained from an water-oil system (\sim 60% TiO₂). ⁶³ The stifled oxidation of Ti₃C₂T_z is likely due to the non-aqueous oil-oil system, as $Ti_3C_2T_z$ nanosheets more readily oxidize in aqueous media.81-83

Armored particles formed from DMF-in-octane emulsions

Armored particles are prepared by the polymerization of the dispersed phase in the oil-oil Pickering emulsions stabilized by modified $Ti_3C_2T_z$. Here, DMF-in-octane emulsions stabilized by DHDAB- $Ti_3C_2T_z$ were used to produce polyurethane particles armored with the modified nanosheets. As is shown in Figure 4A, DMF-in-octane emulsions were first formed in which the dispersed DMF phase contained



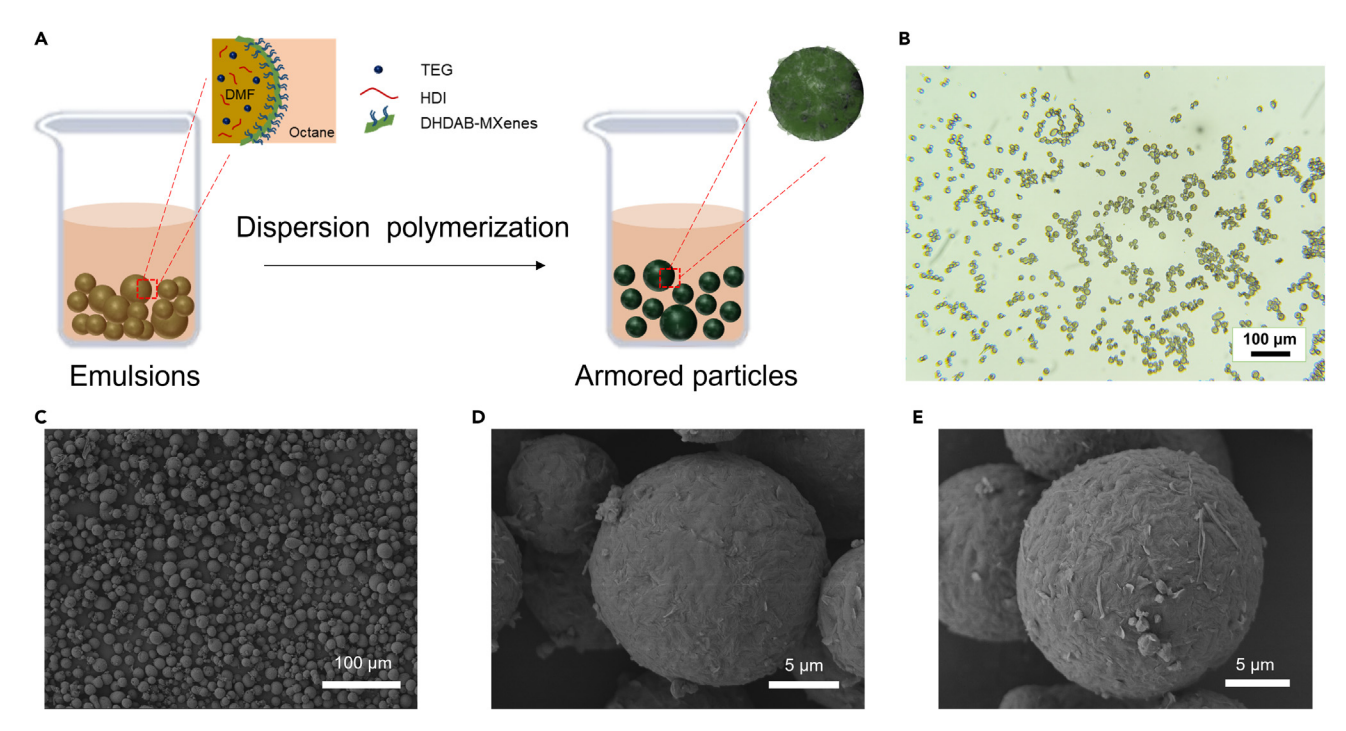


Figure 4. Armored particles from DMF-in-octane emulsions stabilized by DHDAB-Ti₃C₂T_z nanosheets (1 mg/mL, 1:5 v/v of DMF:octane) (A) Synthesis scheme.
(B) Optical microscopy image. Scale bar: 100 μm.

(C–E) SEM images at different magnification. Scale bars: 100 μ m (C), 5 μ m (D and E).

tetra(ethylene glycol) (TEG), HDI, and dibutyltin diacetate (DBTDA) (see "Experimental procedures" for details). Polymerization of the discontinuous phase was initiated by heating the emulsion to 50°C for 5 min. After standing at room temperature for 72 h, the armored particles were characterized by optical microscopy (Figure 4B), which showed distinct spherical particles. The armored particles were isolated by gravity filtration and the structure and morphology were characterized using SEM, which again showed distinct spherical particles with an average size of $\sim\!\!14~\mu\text{m}$ (Figures 4C–4E and S10). In addition, the rough surface of the armored particles indicates the coating of the $Ti_3C_2T_z$ on the surface of the polymer particle. 64

To verify the proposed composition of the DHDAB-Ti₃C₂T_z-coated polyurethane particles, EDS and XPS were used. SEM imaging with elemental mapping of a particle showed uniform distribution of the expected elements, with C, N, O, and Ti observed (Figures 5A-5E). Notably, the Ti elemental mapping indicates the uniform presence of Ti₃C₂T_z nanosheets on the particle surface. The C, N, and O mappings indicate the presence of polyurethane particles. The surface-sensitive technique of XPS supports the presence of the nanosheets on or near the surface, with the survey spectrum also showing a significant Ti 2p peak (Figure 5F). The C, N, and O elements (Table S2) detected from XPS are consistent with the EDS results, and the high-resolution C 1s (Figure S11A) and O 1s (Figure S11B) spectra show the distinct C-N, C-O, and COO peaks, confirming the formation of the polyurethane. In addition, the FTIR spectrum of armored particles shows characteristic N-H stretching $(3,316 \text{ cm}^{-1})$, C-H stretching $(2,921 \text{ and } 2,855 \text{ cm}^{-1})$, C=O stretching (1,683 cm⁻¹), N-H bending (1,534 cm⁻¹), and C-O stretching (1,264 cm⁻¹) peaks, confirming the presence of polyurethane (Figure S12). The high-resolution Ti 2p signal was deconvoluted to Ti-C, Ti²⁺, Ti³⁺, and TiO₂, which confirmed the presence





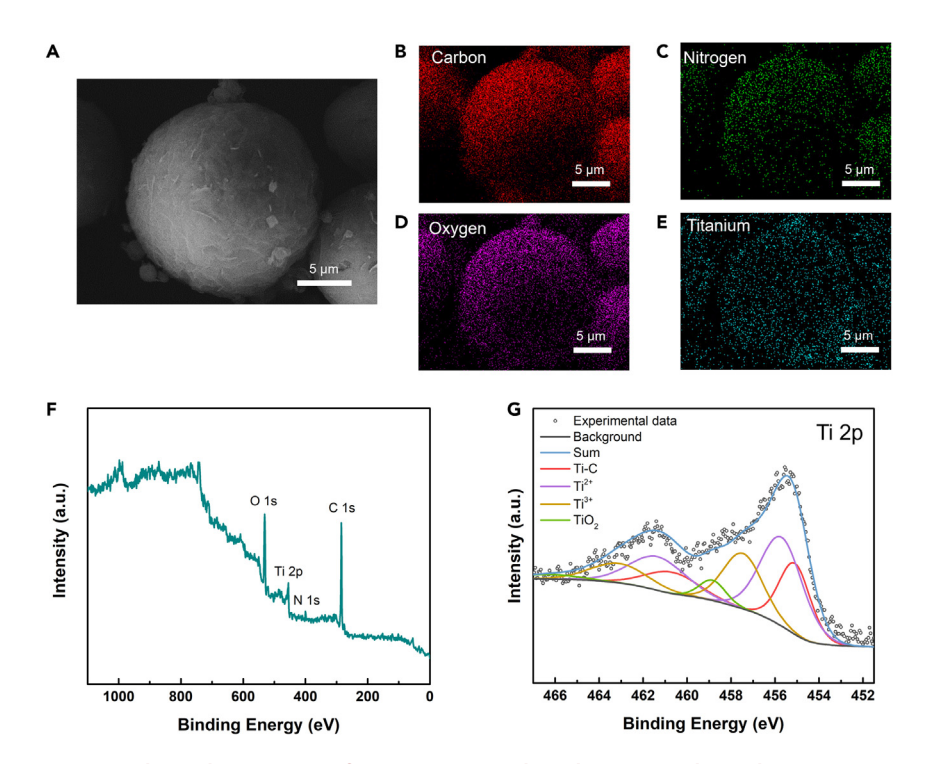


Figure 5. Chemical composition of DHDAB-Ti $_3$ C $_2$ T $_z$ -polyurethane armored particles (A) SEM image. Scale bar: 5 μ m. (B–E) EDS mapping (C, N, O, and Ti) corresponding to the SEM image in (A). Scale bars: 5 μ m. (F) XPS survey spectrum.

(G) Deconvoluted XPS high-resolution Ti 2p peak.

of $Ti_3C_2T_z$. Here, only 6.1% of Ti 2p signal is from TiO_2 (green curve), which suggests little oxidation occurred during the armored particle formation process (i.e., emulsion formation, polymerization, and washing). These results again support that the non-aqueous emulsion can mitigate $Ti_3C_2T_z$ oxidation during structured composite formation.

Porous monolith formed from octane-in-DMF emulsions

The ability to dictate (and have the inverse) oil-oil interface by controlling functionalization of the nanosheets allows the same chemistry to be used for polymerization of the continuous phase rather than the discontinuous phase. To this end, an octanein-DMF emulsion stabilized by OTAB-Ti₃C₂T_z was used to prepare a porous OTAB-Ti₃C₂T_z-polyurethane composite foam. As shown in Figure 6A, HDI and TEG were added to a DMF dispersion of OTAB-Ti₃C₂T_z before octane was added, and the system was agitated to form the octane-in-DMF emulsion. Polymerization of the continuous phase was initiated by heating the sample to 50°C for 5 min. After 72 h, the solid sample was washed and dried to remove the octane droplets, resulting a dark green porous structure, as shown in Figure 6B. A cross section of the porous monolith was characterized by SEM and revealed a closed-cell porous structure with an average pore size of 19.7 μm , as determined by ImageJ analysis (Figures 6C-6E). These voids are formed upon polymerization around the droplets, then removal of the octane trapped during polymerization leads to a porous monoliths structure. As shown in the higher-magnification SEM image of Figure 6E, the pore within the monolith has a rough surface but the polymer surface is smooth, which suggests the Ti₃C₂T_z are coating the pore (Figure 6E). To verify the composition of composite, SEM-EDS was used; elemental mappings of C, N, and O on the



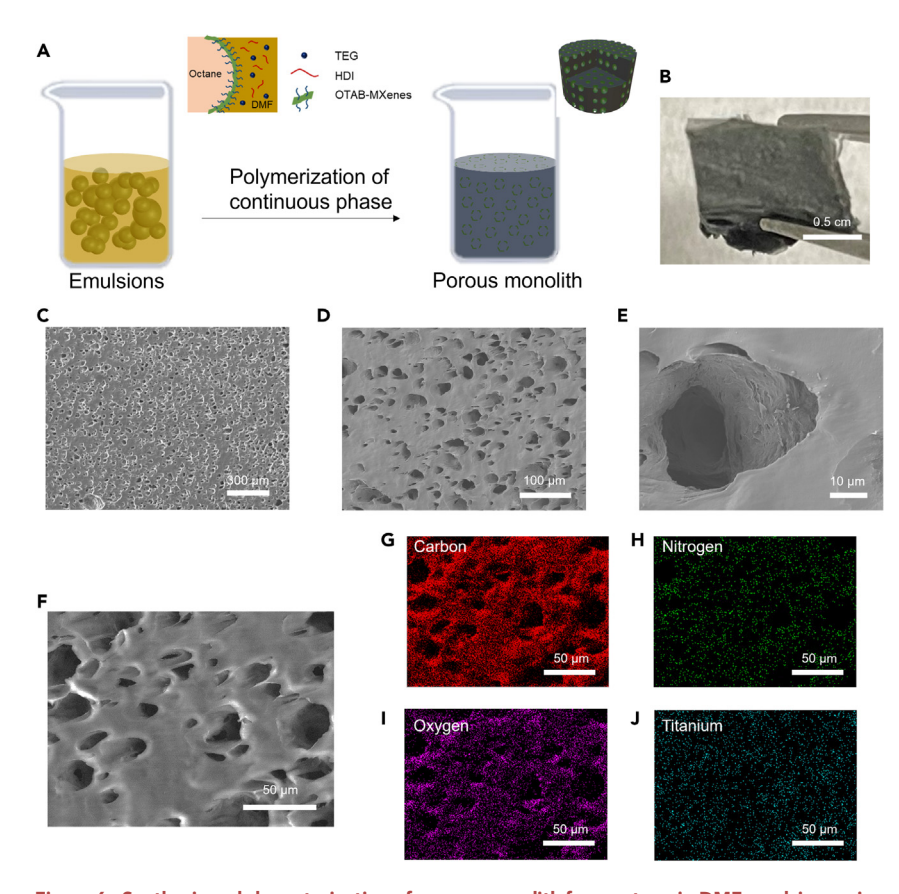


Figure 6. Synthesis and characterization of porous monolith from octane-in-DMF emulsions using OTAB-Ti $_3$ C $_2$ T $_z$ (1 mg/mL, 3:10 v/v of octane:DMF)

(A) Synthetic scheme.

(B) Digital image. Scale bar: 0.5 cm.

(C–F) SEM images of dried porous monolith. Scale bars: $300~\mu m$ (C), $100~\mu m$ (D), $10~\mu m$ (E), $50~\mu m$ (F). (G–J) EDS mapping (C, N, O, and Ti) corresponding to the SEM image in (F). Scale bars: $50~\mu m$.

cross section of the porous monolith supports the presence of polyurethane struts around the pores (Figures 6G–6I). The Ti elemental mapping shown in Figure 6J indicates higher signal in the pores than the polymer strut, also supporting a $\rm Ti_3C_2T_z$ -rich surface of the pores. XPS of the porous monolith shows C, N, O, and Ti elements (Figure S13A; Table S3), indicating the presence of $\rm Ti_3C_2T_z$ -polyurethane. The Ti 2p peak was weak in this case since the penetration depth of XPS was low and the nanosheets were located inside of the pores rather than the sample plane (Figure S8B). The high-resolution C 1s (Figure S14A) and O 1s (Figure S14B) spectra show C–N, C–O, and COO peaks, verifying the formation of polyurethanes. This is also confirmed by the FTIR spectrum of the porous monolith (Figure S15), showing characteristic N–H stretching (3,309 cm $^{-1}$), C–H stretching (2,923 and 2,856 cm $^{-1}$), C=O stretching (1,685 cm $^{-1}$), N–H bending (1,533 cm $^{-1}$), and C–O stretching (1,245 cm $^{-1}$) peaks in the polyurethane. These results confirmed the formation of porous $\rm Ti_3C_2T_z$ -polyurethane monolith with $\rm Ti_3C_2T_z$ mainly located at the pore surface.

In the production of porous monoliths by polymerization of the continuous phase of the oil-oil MXene-stabilized emulsions, the resulting pore size and pore concentration are dictated by the emulsion droplet size, which can be tuned by the relative volume of the inner phase. A 3:10 (v/v) ratio of octane/DMF was first used for the





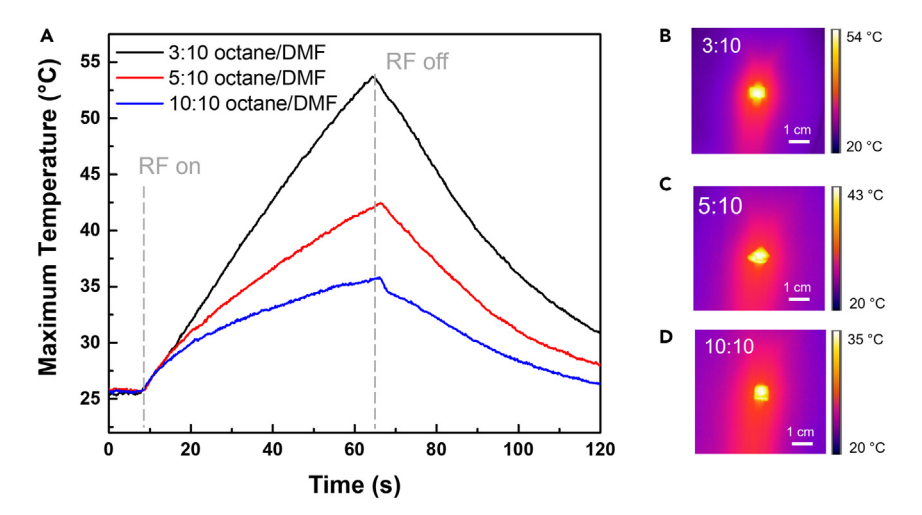


Figure 7. RF heating behavior (1 W, 135 MHz) of OTAB- $Ti_3C_2T_z$ porous monolith with different ratios of octane/DMF (v/v)

- (A) The maximum temperature of the porous monolith versus time (black, 3:10; red, 5:10; blue,
- 10:10). The trend shows heating rate increases as void fraction decreases.
- (B) Thermal image of the monolith with 3:10 octane/DMF ratio. Scale bar: 1 cm.
- (C) Thermal image of the monolith with 5:10 octane/DMF ratio. Scale bar: 1 cm.
- (D) Thermal image of the monolith with 10:10 octane/DMF ratio. Scale bar: 1 cm.

emulsion formation, resulting small and mostly closed pores (average size, $\sim \! 19.7~\mu m$; Figures 6C–6E). For comparison, an increased octane/DMF ratio (5:10, v/v) was also used for the formation of OTAB-Ti $_3$ C $_2$ T $_z$ -polyurethane porous monolith (Figures S16A–S16C); as expected, larger pores were observed (average diameter of 27.2 μm). The enlarged pores are due to increased octane volume but consistent amount of nanosheet and thus interfacial area. Preparing monoliths with a volume ratio of octane/DMF 10:10 (v/v), the pore size within the monolith further increases to 40.6 μm (Figures S16D–S16E). The pore size distribution based on oil/oil volume, as shown in Figure S17, confirms the trend that larger pores correlate to higher internal volume phase percentage. In addition, the higher internal volume dictates higher void fraction of the monolith. For example, the void fraction of the porous monoliths with 3:10, 5:10, and 10:10 octane/DMF ratios is 36.8%, 50.7%, and 57.0%, respectively (Table S4).

One of the distinctive properties of MXenes is the rapid heating performance under electromagnetic field due to the strong absorption of EM waves and high dielectric loss tangent.80 To demonstrate this unique RF heating property of our emulsiontemplated structured Ti₃C₂T_z-polymer composites, we performed RF heating tests on the porous OTAB-Ti₃C₂T_z-polyurethane foam. When exposed to electromagnetic fields in the MHz range, the closed cells of Ti₃C₂T_z nanosheets within the polyurethane foam absorb field energy and dissipate power as heat. To set up the experiments, the porous Ti₃C₂T₇-polyurethane monoliths of various void fraction were exposed to an RF field, and the change in temperature of the composite was measured with a thermal camera. The field was generated via a coplanar fringingfield applicator and maintained at 1 W and 135 MHz. For these samples, the initial heating rate was similar but, over 60-s period, the heating rate increased with a decrease in void fraction (Figures 7A-7D). For example, the sample made with a 3:10 octane/DMF ratio heated steadily to 54°C after being exposed for 60 s. In comparison, samples with 5:10 and 10:10 octane/DMF ratios heated slower, reaching 43°C and 35°C after 60 s, respectively. This trend is affected both by local electrically Please cite this article in press as: Cao et al., Structured $T_{i_3}C_2T_z$ MXene-polymer composites from non-aqueous emulsions, Matter (2024), https://doi.org/10.1016/j.matt.2024.02.011





conductive regions as well as the bulk thermal conductivity of the sample. Pore size may affect the conductive regions and their placement near the pores, and the thermal conductivity affects how heat dissipates throughout the sample. The less porous sample (e.g., 3:10 octane/DMF sample) has smaller and more closed pores and higher density, which may have more local conductive regions, resulting in higher heating performance. Moreover, the samples with more voids conduct heat slower (Figure S18), which may account for the heating difference in response to RF.

Conclusions

We have reported a feasible method to prepare non-aqueous emulsions stabilized by modified Ti₃C₂T₇ MXene nanosheets and their use in templating structured polymer composites for selective polymerization of the continuous phase or discontinuous phase or interfacial polymerization. By controlling the wettability of modified $Ti_3C_2T_z$, DHDAB- $Ti_3C_2T_z$ and OTAB- $Ti_3C_2T_z$ nanosheets stabilize DMF-in-octane and octane-in-DMF emulsions, respectively. Selective solubility of monomers allows for subsequent polymerization within the emulsions and the fabrication of structured polymer composites. The morphology of the three structures of ${\rm Ti}_3{\rm C}_2{\rm T}_z$ -polyurea capsules by interfacial polymerization, Ti₃C₂T_z armored polyurethane particles by dispersion polymerization, and porous $Ti_3C_2T_2$ -polyurethane monoliths by polymerization of the continuous phase were confirmed by optical microscopy and SEM. The presence of the polymer and Ti₃C₂T_z nanosheets were verified by SEM-EDS and XPS, as was localization of the nanosheets at the interfaces and the limited extent of nanosheet oxidation. We highlight that the porous Ti₃C₂T_z-polyurethane monolith exhibits rapid and steady heating in response to RF field at low power (1 W, 135 MHz). The method presented herein provides a simple approach to produce solution-processable MXene nanosheets that stabilize oil-oil emulsions and their use to make structured MXene-polymer composites. The development of the nonaqueous system enables water-sensitive and/or water-miscible reagents and solvents to be used and coupled with polymerization within emulsions, which expands the range of accessible MXene-polymer composites with tailorable compositions to include, e.g., salt hydrates, ionic liquids, and deep eutectic solvents. Importantly, this approach enables the use of particle surfactants that are both solution processable and have functional properties (e.g., conductive, catalytic, optical) such that functional composites can be made in a single step, without the need for post-processing, such as chemical or thermal treatment. Indeed, structured polymer composites containing MXenes will find application in energy management, antibacterial coatings, catalysis, carbon capture, remediation, and sensing (Figure S19).

EXPERIMENTAL PROCEDURES

Resource availability

Lead contact

Further information and requests for resources and reagents should be directed to and will be fulfilled by the lead contact, Micah J. Green (micah.green@tamu.edu).

Materials availability

This study did not generate new unique reagents.

Data and code availability

This study did not generate datasets.

Materials

The Ti_3AIC_2 MAX phase was prepared as previously reported. ⁸¹ LiF (98%+) was purchased from Alfa Aesar. HCI (37% [w/w], ACS reagent), DMSO (>99.5%), EDA, HDI,

Please cite this article in press as: Cao et al., Structured $Ti_3C_2T_z$ MXene-polymer composites from non-aqueous emulsions, Matter (2024), https://doi.org/10.1016/j.matt.2024.02.011





DHDAB, and DBTDA were purchased from Sigma-Aldrich. DMF (anhydrous), OTAB, and TEG were purchased from Fisher Scientific. All reagents were used as received, without further purification.

Instrumentation

Emulsions were made using a handheld emulsifier from BioSpec Products (model 985370). Optical microscopy images were obtained using an Amscope microscope. Samples for optical microscopy visualization were prepared by placing a drop of emulsion solution onto a glass slide. XRD was conducted on a Miniflex II (Rigaku) with Cu-K α radiation source (λ = 1.5406 Å), XPS was performed using an Omicron X-ray photoelectron spectrometer employing an Mg-sourced X-ray beam at 15 kV with aperture 3. FTIR spectroscopy was performed on a JASCO FTIR spectrometer, model FTIR-4600LE MidIR. TEM was performed using an FEI Tecnai F20 transmission electron microscope operating at 200 kV. SEM was performed on an FEI Quanta 600 field-emission scanning electron microscope with the acceleration voltage of 5 and 20 kV for imaging and EDS analysis, respectively. The SEM samples were coated with 3-nm platinum to avoid charging issues. The contrast of EDS mapping images was enhanced for better visibility. Water contact measurements were conducted using a KSV Cam 200 Goniometer (Espoo, Finland) and a sessile drop method with 5-μL droplets. TGA was conducted on a TA instrument Q50 under nitrogen flow. RF heating measurements were conducted using a signal generator (Rigol, DSG815), an amplifier (Mini-Circuits, ZHL-100W-GAN+), and a fringing-field applicator (HFSS, ANSYS). The temperature was monitored by a thermal camera (FLIR Systems, A655sc). The size distribution of armored particles and porous monolith were calculated using ImageJ on the SEM images (>100 data points for each size analysis).

Preparation of Ti₃C₂T_z nanosheets

 $T_{i3}C_2T_z$ nanosheets were obtained following our previously reported method. ^{81,84} Briefly, 1.6 g of LiF was added to 20 mL of 6 M aqueous HCl solution with continuous stirring. Next, 2 g of MAX powder was slowly added to this solution and the mixture stirred continuously at 40° C for 40 h. The resulting suspension was washed with deionized water and separated by centrifugation with the supernatant discarded. This washing process was repeated until the supernatant reached pH \sim 6, as determined by litmus paper. Then, the precipitate ($T_{i3}C_2T_z$ clay) was dispersed and intercalated with DMSO at room temperature for 20 h while stirring. Excess DMSO was removed by centrifugation (supernatant discarded) followed by washing with deionized water thrice with centrifugation at 9,000 rpm for 30 min, discarding the supernatant. Then, the precipitate was dispersed in fresh water and bath sonicated for 1 h. Aqueous dispersion of $T_{i3}C_2T_z$ nanosheets was obtained by centrifuging the suspension at 3,500 rpm for 45 min and collecting the supernatant.

Functionalization of Ti₃C₂T_z

To prepare modified $Ti_3C_2T_z$, two small molecules (DHDAB and OTAB) were used, and a similar procedure was followed for each. DHDAB- $Ti_3C_2T_z$ were obtained by first adding 30 mg of DHDAB dissolved in a 15-mL water/ethanol (v/v, 80:20) mixture to 15 mL of $Ti_3C_2T_z$ water/ethanol (80:20) dispersion (2 mg/mL) and then stirred overnight. The resulting suspension was washed three times in a water/ethanol (80:20) mixture and three times with ethanol and then centrifuged to remove excess DHDAB. To make DHDAB- $Ti_3C_2T_z$ dispersion in octane, a solvent exchange method was used. The as-prepared DHDAB- $Ti_3C_2T_z$ was washed with three times in octane to remove residue ethanol and then dispersed in octane to make a 2-mg/mL dispersion. OTAB- $Ti_3C_2T_z$ were obtained in a similar way. The washing steps might also wash off loosely attached small molecules (DHDAB or OTAB), and the



characterization of the modified $Ti_3C_2T_z$ nanosheets was conducted after the washing and drying steps. In addition, different ratios (including 0.35:1 and 0.5:1) of small molecules (DHDAB and OTAB) to $Ti_3C_2T_z$ were also prepared using the same method. A ratio of 1:1 (small molecule to $Ti_3C_2T_z$) was selected for the composite formation in our paper based on the emulsion quality (dark aggregates are observed in the other two ratios of 0.35:1 and 0.5:1, as seen in Figures S20 and S21).

Preparation of modified Ti₃C₂T_z-stabilized oil-in-oil emulsions

Modified $Ti_3C_2T_z$ -stabilized emulsions were prepared as follows. First, two immiscible oil phases were prepared. To make DMF-in-octane emulsions, 1 mL of 1 mg/mL DHDAB- $Ti_3C_2T_z$ in octane dispersion was used as the continuous phase and 0.2 mL of DMF was added, followed by homogenizing using a handheld emulsifier for 1 min. To make the inverse octane-in-DMF emulsions, OTAB- $Ti_3C_2T_z$ was used, and the emulsions were formed in a similar way.

Preparation of DHDAB-Ti₃C₂T_z capsules

DHDAB- ${\rm Ti_3C_2T_z}$ capsules were obtained by interfacial polymerization in Pickering emulsions. The dispersed phase consisted of 0.2 mL of DMF and 0.05 mmol of EDA. The (DMF/EDA)-in-octane emulsions were formed by mixing the dispersed phase with 1 mL of DHDAB- ${\rm Ti_3C_2T_z}$ octane dispersion. Then, 0.05 mmol of HDI in 0.1 mL of octane solution was dropwise added to the continuous phase of the emulsions with hand shaking. The mixture was stored at room temperature for 72 h. The capsules were obtained by gravity filtration and washing with hexanes several times. The isolated capsules were dried and stored in a vacuum oven for further analysis. Note that, in order to better see the hollow features of the capsules, the samples were harshly treated when preparing SEM samples.

Preparation of DHDAB- $Ti_3C_2T_z$ armored particles

DHDAB- $Ti_3C_2T_z$ armored particles were obtained by dispersion polymerization in Pickering emulsions. Two monomers (0.5 mmol of HDI and 0.5 mmol of TEG) were dissolved in 50 μ L of DMF as the dispersed phase and 2 μ L of DBTDA was then added. All the reagents (DMF, monomers, and DBTDA) were stored and cooled in the fridge before mixing. Then, emulsions were formed by mixing the dispersed phase with a 1-mL DHDAB- $Ti_3C_2T_z$ octane dispersion. The resulting suspension was first heated to 50°C for 5 min to start the polymerization. Then, after 72-h reaction at room temperature, the armored particles were isolated using gravity filtration and washed with hexanes several times. The armored particles were dried and stored in a vacuum oven for further analysis.

Preparation of OTAB-Ti₃C₂T_z porous monolith

OTAB- $Ti_3C_2T_z$ porous monoliths were obtained by polymerizing the continuous phase of Pickering emulsions. The dispersed phase consisted of 0.3 mL of octane. The continuous phase consisted of 1 mg/mL OTAB- $Ti_3C_2T_z$, 0.46 mL of DMF, 1.6 mmol of HDI, 1.6 mmol of TEG, and 5 μ L of DBTDA (last added). All the reagents (DMF, monomers, and DBTDA) were stored in the fridge before mixing. Then octane-in-DMF emulsions were formed by homogenizing the mixture of dispersed phase and continuous phase. The resulting suspension was heated to 50°C for 5 min to initiate the polymerization and then stored at room temperature for 72 h. The porous monolith was then obtained by washing with hexanes and ethanol before drying in the vacuum oven.





SUPPLEMENTAL INFORMATION

Supplemental information can be found online at https://doi.org/10.1016/j.matt. 2024.02.011.

ACKNOWLEDGMENTS

The authors thank Texas A&M University for financial support. E.P. thanks NSF DMR CAREER award #2103182. M.G., M.R., and J.L.L. thank NSF CMMI award #2240554. We would like to thank TAMU Materials Characterization Facilities for use of XPS, SEM, and EDS and the Microscopy and Imaging Center for use of TEM. Use of the Texas A&M University Soft Matter Facility for TGA is acknowledged. We thank Dr. Pentzer group student Chia-Min Hsieh for the help collecting TGA data. We also thank Dr. Mustafa Akbulut's group and graduate students Shuhao Liu and Wentao Zhou at Texas A&M University for their help in the use of the Zetasizer instrument and contact angle measurement. We acknowledge the help from Xiaofei Zhao in the synthesis process of MXenes.

AUTHOR CONTRIBUTIONS

The manuscript was written with contributions of all authors. H.C. conducted experiments (MXene synthesis, MXene functionalization, emulsion preparation, and polymerization), collected characterization data and analysis, and wrote the manuscript. Y.W. helped with emulsion and polymerization experiments and data analysis. Z.T. synthesized the MAX phase and helped with MXene synthesis. E.H. and S.D. conducted RF heating experiments and data analysis. J.L.L. and M.R. revised the manuscript and provided critical feedback. E.B.P. and M.J.G. supervised the project. All authors have given approval to the final version of the manuscript.

DECLARATION OF INTERESTS

The authors declare no competing interests.

Received: October 6, 2023 Revised: January 24, 2024 Accepted: February 16, 2024 Published: March 12, 2024

REFERENCES

- Jordan, J., Jacob, K.I., Tannenbaum, R., Sharaf, M.A., and Jasiuk, I. (2005). Experimental trends in polymer nanocomposites—a review. Mater. Sci. Eng. 393, 1–11. https://doi.org/10.1016/j. msea.2004.09.044.
- 2. Carey, M., and Barsoum, M.W. (2021). MXene polymer nanocomposites: a review. Materials Today Advances 9, 100120. https://doi.org/10.1016/j.mtadv.2020.100120.
- 3. Naguib, M., Saito, T., Lai, S., Rager, M.S., Aytug, T., Parans Paranthaman, M., Zhao, M.-Q., and Gogotsi, Y. (2016). Ti3C2Tx (MXene)–polyacrylamide nanocomposite films. RSC Adv. 6, 72069–72073. https://doi.org/10. 1039/C6R410384G
- Mirkhani, S.A., Shayesteh Zeraati, A., Aliabadian, E., Naguib, M., and Sundararaj, U. (2019). High Dielectric Constant and Low Dielectric Loss via Poly(vinyl alcohol)/Ti3C2Tx MXene Nanocomposites. ACS Appl. Mater. Interfaces 11, 18599–18608. https://doi.org/10. 1021/acsami.9b00393.
- Shamsabadi, A.A., Isfahani, A.P., Salestan, S.K., Rahimpour, A., Ghalei, B., Sivaniah, E., and Soroush, M. (2020). Pushing Rubbery Polymer Membranes To Be Economic for CO2 Separation: Embedment with Ti3C2Tx MXene Nanosheets. ACS Appl. Mater. Interfaces 12, 3984–3992. https://doi.org/10.1021/acsami. 9b19960.
- Alfred, A., Jamari, S.S., Mariatti, M., and Ghazali, S. (2023). Segregated nanofiller: Recent development in polymer-based composites and its applications. Mater. Today: Proc. https://doi.org/10.1016/j.matpr.2023. 05 120
- Liao, Z., Zhu, J., Li, X., and Van der Bruggen, B. (2021). Regulating composition and structure of nanofillers in thin film nanocomposite (TFN) membranes for enhanced separation performance: A critical review. Separ. Purif. Technol. 266, 118567. https://doi.org/10.1016/ j.seppur.2021.118567.
- Zhang, Q., Wang, Q., Cui, J., Zhao, S., Zhang, G., Gao, A., and Yan, Y. (2023). Structural design and preparation of Ti3C2Tx MXene/ polymer composites for absorptiondominated electromagnetic interference shielding. Nanoscale Adv. 5, 3549–3574. https://doi.org/10.1039/D3NA00130J.
- Ma, W., Cai, W., Chen, W., Liu, P., Wang, J., and Liu, Z. (2021). Microwave-induced segregated composite network with MXene as interfacial solder for ultra-efficient electromagnetic interference shielding and anti-dripping. Chem. Eng. J. 425, 131699. https://doi.org/10. 1016/j.cej.2021.131699.
- Wang, Y., Li, Y., Wang, L., Yuan, Q., Chen, J., Niu, Y., Xu, X., Wang, Q., and Wang, H. (2020). Gradient-layered polymer nanocomposites with significantly improved insulation performance for dielectric energy storage. Energy Storage Mater. 24, 626–634. https:// doi.org/10.1016/j.ensm.2019.06.013.



- Echols, I.J., An, H., Yun, J., Sarang, K.T., Oh, J.-H., Habib, T., Zhao, X., Cao, H., Holta, D.E., Radovic, M., et al. (2021). Electronic and Optical Property Control of Polycation/MXene Layer-by-Layer Assemblies with Chemically Diverse MXenes. Langmuir 37, 11338–11350. https://doi.org/10.1021/acs.langmuir.1c01904.
- Gao, Q., Pan, Y., Zheng, G., Liu, C., Shen, C., and Liu, X. (2021). Flexible multilayered MXene/thermoplastic polyurethane films with excellent electromagnetic interference shielding, thermal conductivity, and management performances. Adv. Compos. Hybrid Mater. 4, 274–285. https://doi.org/10. 1007/s42114-021-00221-4.
- Zhang, X., Xu, Y., Zhang, X., Wu, H., Shen, J., Chen, R., Xiong, Y., Li, J., and Guo, S. (2019). Progress on the layer-by-layer assembly of multilayered polymer composites: Strategy, structural control and applications. Prog. Polym. Sci. 89, 76–107. https://doi.org/10. 1016/j.progpolymsci.2018.10.002.
- Wei, B., Chen, X., and Yang, S. (2021). Construction of a 3D aluminum flake framework with a sponge template to prepare thermally conductive polymer composites.
 J. Mater. Chem. A Mater. 9, 10979–10991. https://doi.org/10.1039/DOTA12541E.
- Karger-Kocsis, J., Mahmood, H., and Pegoretti, A. (2015). Recent advances in fiber/matrix interphase engineering for polymer composites. Prog. Mater. Sci. 73, 1–43. https:// doi.org/10.1016/j.pmatsci.2015.02.003.
- Wang, Y., Peng, H.-K., Li, T.-T., Shiu, B.-C., Ren, H.-T., Zhang, X., Lou, C.-W., and Lin, J.-H. (2021). MXene-coated conductive composite film with ultrathin, flexible, self-cleaning for high-performance electromagnetic interference shielding. Chem. Eng. J. 412, 128681. https://doi.org/10.1016/j.cej.2021. 128681.
- Zeng, Z.-H., Wu, N., Wei, J.-J., Yang, Y.-F., Wu, T.-T., Li, B., Hauser, S.B., Yang, W.-D., Liu, J.-R., and Zhao, S.-Y. (2022). Porous and Ultra-Flexible Crosslinked MXene/Polyimide Composites for Multifunctional Electromagnetic Interference Shielding. Nano-Micro Lett. 14, 59. https://doi.org/10.1007/ s40820-022-00800-0.
- Jin, L., Cao, W., Wang, P., Song, N., and Ding, P. (2022). Interconnected MXene/Graphene Network Constructed by Soft Template for Multi-Performance Improvement of Polymer Composites. Nano-Micro Lett. 14, 133. https:// doi.org/10.1007/s40820-022-00877-7.
- Zhang, F., Feng, Y., and Feng, W. (2020). Threedimensional interconnected networks for thermally conductive polymer composites: Design, preparation, properties, and mechanisms. Mater. Sci. Eng. R Rep. 142, 100580. https://doi.org/10.1016/j.mser.2020. 100580.
- Wang, D., Lin, Y., Hu, D., Jiang, P., and Huang, X. (2020). Multifunctional 3D-MXene/PDMS nanocomposites for electrical, thermal and triboelectric applications. Compos. Appl. Sci. Manuf. 130, 105754. https://doi.org/10.1016/j. compositesa.2019.105754.
- Fujisawa, S. (2021). Material design of nanocellulose/polymer composites via Pickering emulsion templating. Polym. J. 53,

- 103–109. https://doi.org/10.1038/s41428-020-00408-4.
- Bago Rodriguez, A.M., and Binks, B.P. (2019). Capsules from Pickering emulsion templates. Curr. Opin. Colloid Interface Sci. 44, 107–129. https://doi.org/10.1016/j.cocis.2019.09.006.
- Zhu, H., Lei, L., Li, B.-G., and Zhu, S. (2018). Development of Novel Materials from Polymerization of Pickering Emulsion Templates. In Polymer Reaction Engineering of Dispersed Systems, Volume I, W. Pauer, ed. (Springer International Publishing), pp. 101–119. https://doi.org/10.1007/ 12_2017_15.
- Werner, A., Sèbe, G., and Héroguez, V. (2018). A new strategy to elaborate polymer composites via Pickering emulsion polymerization of a wide range of monomers. Polym. Chem. 9, 5043–5050. https://doi.org/ 10.1039/C8PY01022F.
- Pentzer, E., Cruz Barrios, E., and Starvaggi, N. (2023). Pickering Emulsions as Templates for Architecting Composite Structures. Acc. Mater. Res. 4, 641–647. https://doi.org/10. 1021/accountsmr.3c00058.
- Huo, J., Marcello, M., Garai, A., and Bradshaw, D. (2013). MOF-Polymer Composite Microcapsules Derived from Pickering Emulsions. Adv. Mater. 25, 2717–2722. https:// doi.org/10.1002/adma.201204913.
- Lotierzo, A., and Bon, S.A.F. (2017). A mechanistic investigation of Pickering emulsion polymerization. Polym. Chem. 8, 5100–5111. https://doi.org/10.1039/ C7PY00308K.
- Hu, Y., Wang, J., Li, X., Hu, X., Zhou, W., Dong, X., Wang, C., Yang, Z., and Binks, B.P. (2019). Facile preparation of bioactive nanoparticle/ poly(e-caprolactone) hierarchical porous scaffolds via 3D printing of high internal phase Pickering emulsions. J. Colloid Interface Sci. 545, 104–115. https://doi.org/10.1016/j.jcis. 2019.03.024.
- Yao, C., Shi, G., Hu, Y., Zhuo, H., Chen, Z., Peng, X., Zhong, L., and Liu, C. (2021). Emulsion templated advanced functional materials from emerging nano building blocks. J. Mater. Chem. A Mater. 9, 25827–25851. https://doi. org/10.1039/D1TA05420A.
- Li, C., Li, H., Tan, J., Xue, Y., Liu, Q., Yang, Y., Wang, C., and Zhang, Q. (2022). Constructing segregated thermoset composite via Pickering emulsion and dynamic polythiourethanes. Compos. Sci. Technol. 218, 109215. https://doi. org/10.1016/j.compscitech.2021.109215.
- Yu, B., Zhao, Z., Fu, S., Meng, L., Liu, Y., Chen, F., Wang, K., and Fu, Q. (2019). Fabrication of PLA/CNC/CNT conductive composites for high electromagnetic interference shielding based on Pickering emulsions method. Compos. Appl. Sci. Manuf. 125, 105558. https://doi.org/10.1016/j.compositesa.2019. 105558.
- Yang, Z., Liu, H., Wu, S., Tang, Z., Guo, B., and Zhang, L. (2018). A green method for preparing conductive elastomer composites with interconnected graphene network via Pickering emulsion templating. Chem. Eng. J. 342, 112–119. https://doi.org/10.1016/j.cej. 2018.02.079.

- Brunier, B., Sheibat-Othman, N., Chniguir, M., Chevalier, Y., and Bourgeat-Lami, E. (2016). Investigation of Four Different Laponite Clays as Stabilizers in Pickering Emulsion Polymerization. Langmuir 32, 6046-6057. https://doi.org/10.1021/acs.langmuir.6b01080.
- Machado, J.P.E., de Freitas, R.A., and Wypych, F. (2019). Layered clay minerals, synthetic layered double hydroxides and hydroxide salts applied as pickering emulsifiers. Appl. Clay Sci. 169, 10–20. https://doi.org/10.1016/j.clay.2018. 12.007.
- Qiao, X.G., Dugas, P.Y., Prevot, V., and Bourgeat-Lami, E. (2020). Surfactant-free synthesis of layered double hydroxidearmored latex particles. Polym. Chem. 11, 3195–3208. https://doi.org/10.1039/ D0PY00140F.
- Wu, C., Hou, D., Yin, B., and Li, S. (2022). Synthesis and application of new core-shell structure via Pickering emulsion polymerization stabilized by graphene oxide. Compos. B Eng. 247, 110285. https://doi.org/10.1016/j. compositesb.2022.110285.
- Yin, G., Zheng, Z., Wang, H., Du, Q., and Zhang, H. (2013). Preparation of graphene oxide coated polystyrene microspheres by Pickering emulsion polymerization. J. Colloid Interface Sci. 394, 192–198. https://doi.org/10.1016/j. icis.2012.11.024.
- 38. Escamilla, M., Pachuta, K., Huang, K., Klingseisen, M., Cao, H., Zhang, H., Sehirlioglu, A., and Pentzer, E. (2022). Polymer particles armored with cobalt oxide nanosheets for the catalytic degradation of bisphenol A. Mater. Adv. 3, 2354–2363. https://doi.org/10.1039/
- Luo, Q., Wang, Y., Chen, Z., Wei, P., Yoo, E., and Pentzer, E. (2019). Pickering Emulsion-Templated Encapsulation of Ionic Liquids for Contaminant Removal. ACS Appl. Mater. Interfaces 11, 9612–9620. https://doi.org/10. 1021/acsami.8b21881.
- Luo, Q., Wei, P., and Pentzer, E. (2016). Hollow microcapsules by stitching together of graphene oxide nanosheets with a difunctional small molecule. Carbon 106, 125–131. https://doi.org/10.1016/j.carbon. 2016.05.024.
- Edgehouse, K., Escamilla, M., Wang, L., Dent, R., Pachuta, K., Kendall, L., Wei, P., Sehirlioglu, A., and Pentzer, E. (2019). Stabilization of oil-inwater emulsions with graphene oxide and cobalt oxide nanosheets and preparation of armored polymer particles. J. Colloid Interface Sci. 541, 269–278. https://doi.org/10.1016/j. jcis.2019.01.092.
- Xie, P., Ge, X., Fang, B., Li, Z., Liang, Y., and Yang, C. (2013). Pickering emulsion polymerization of graphene oxide-stabilized styrene. Colloid Polym. Sci. 291, 1631–1639. https://doi.org/10.1007/s00396-013-2897-x.
- 43. Yang, L., Jiang, C., Yan, J., Shen, Y., Chen, Y., Xu, L., and Zhu, H. (2020). Structuring the reduced graphene oxide/polyHIPE foam for piezoresistive sensing via emulsion-templated polymerization. Compos. Appl. Sci. Manuf. 134, 105898. https://doi.org/10.1016/j. compositesa.2020.105898.



- Ghidiu, M., Lukatskaya, M.R., Zhao, M.-Q., Gogotsi, Y., and Barsoum, M.W. (2014). Conductive two-dimensional titanium carbide 'clay' with high volumetric capacitance. Nature 516, 78–81. https://doi.org/10.1038/ nature13970
- Naguib, M., Kurtoglu, M., Presser, V., Lu, J., Niu, J., Heon, M., Hultman, L., Gogotsi, Y., and Barsoum, M.W. (2011). Two-Dimensional Nanocrystals Produced by Exfoliation of Ti3AIC2. Adv. Mater. 23, 4248–4253. https:// doi.org/10.1002/adma.201102306.
- Naguib, M., Mochalin, V.N., Barsoum, M.W., and Gogotsi, Y. (2014). 25th Anniversary Article: MXenes: A New Family of Two-Dimensional Materials. Adv. Mater. 26, 992–1005. https:// doi.org/10.1002/adma.201304138.
- 47. Naguib, M., Barsoum, M.W., and Gogotsi, Y. (2021). Ten Years of Progress in the Synthesis and Development of MXenes. Adv. Mater. 33, 2103393. https://doi.org/10.1002/adma. 202103393
- Shahzad, F., Alhabeb, M., Hatter, C.B., Anasori, B., Man Hong, S., Koo, C.M., and Gogotsi, Y. (2016). Electromagnetic interference shielding with 2D transition metal carbides (MXenes). Science 353, 1137–1140. https://doi.org/10. 1126/science.aag2421.
- Sun, R., Zhang, H.-B., Liu, J., Xie, X., Yang, R., Li, Y., Hong, S., and Yu, Z.-Z. (2017). Highly Conductive Transition Metal Carbide/ Carbonitride(MXene)@polystyrene Nanocomposites Fabricated by Electrostatic Assembly for Highly Efficient Electromagnetic Interference Shielding. Adv. Funct. Mater. 27, 1702807. https://doi.org/10.1002/adfm. 201702807.
- Song, P., Liu, B., Qiu, H., Shi, X., Cao, D., and Gu, J. (2021). MXenes for polymer matrix electromagnetic interference shielding composites: A review. Compos. Commun. 24, 100653. https://doi.org/10.1016/j.coco.2021. 100653.
- Morales-García, Á., Calle-Vallejo, F., and Illas, F. (2020). MXenes: New Horizons in Catalysis. ACS Catal. 10, 13487–13503. https://doi.org/ 10.1021/acscatal.0c03106.
- Gao, G., O'Mullane, A.P., and Du, A. (2017). 2D MXenes: A New Family of Promising Catalysts for the Hydrogen Evolution Reaction. ACS Catal. 7, 494–500. https://doi.org/10.1021/ acscatal.6b02754.
- 53. Xia, C., Ye, H., Kim, A., Sabahi Namini, A., Li, S., Delbari, S.A., Park, J.Y., Kim, D., Le, Q.V., Varma, R.S., et al. (2023). Recent catalytic applications of MXene-based layered nanomaterials. Chemosphere 325, 138323. https://doi.org/10.1016/j.chemosphere.2023. 138323.
- Persson, P.O.Å., and Rosen, J. (2019). Current state of the art on tailoring the MXene composition, structure, and surface chemistry. Curr. Opin. Solid State Mater. Sci. 23, 100774. https://doi.org/10.1016/j.cossms.2019.100774.
- Wang, J., Du, C.-F., Xue, Y., Tan, X., Kang, J., Gao, Y., Yu, H., and Yan, Q. (2021). MXenes as a versatile platform for reactive surface modification and superior sodium-ion storages. Exploration 1, 20210024. https://doi. org/10.1002/EXP.20210024.

- Shi, S., Qian, B., Wu, X., Sun, H., Wang, H., Zhang, H.-B., Yu, Z.-Z., and Russell, T.P. (2019). Self-Assembly of MXene-Surfactants at Liquid-Liquid Interfaces: From Structured Liquids to 3D Aerogels. Angew. Chem., Int. Ed. Engl. 58, 18171–18176. https://doi.org/10.1002/anie. 201908402.
- Zhao, S., Li, L., Zhang, H.-B., Qian, B., Luo, J.-Q., Deng, Z., Shi, S., Russell, T.P., and Yu, Z.-Z. (2020). Janus MXene nanosheets for macroscopic assemblies. Mater. Chem. Front. 4, 910–917. https://doi.org/10.1039/ C9QM00681H.
- Zhi, W., Xiang, S., Bian, R., Lin, R., Wu, K., Wang, T., and Cai, D. (2018). Study of MXene-filled polyurethane nanocomposites prepared via an emulsion method. Compos. Sci. Technol. 168, 404–411. https://doi.org/10.1016/j. compscitech.2018.10.026.
- Cao, H., Wang, Y., Sarmah, A., Liu, K.-W., Tan, Z., Arole, K.D., Lutkenhaus, J.L., Radovic, M., Green, M.J., and Pentzer, E.B. (2022). Electrically conductive porous Ti3C2Tx MXenepolymer composites from high internal phase emulsions (HIPEs). 2D Mater. 9, 044004. https:// doi.org/10.1088/2053-1583/ac914c.
- Han, X., Qiu, X., Zong, M., and Hao, J. (2023). Assembled MXene Macrostructures for Multifunctional Polymer Nanocomposites (Small Structures n/a), pp. 2300090. https://doi. org/10.1002/sstr.202300090.
- Zheng, Z., Zhao, Y., Ye, Z., Hu, J., and Wang, H. (2022). Electrically conductive porous MXenepolymer composites with ultralow percolation threshold via Pickering high internal phase emulsion templating strategy. J. Colloid Interface Sci. 618, 290–299. https://doi.org/10. 1016/j.jcis.2022.03.086.
- 62. Fan, Q., Yi, M., Chai, C., Li, W., Qi, P., Wang, J., and Hao, J. (2022). Oxidation stability enhanced MXene-based porous materials derived from water-in-ionic liquid Pickering emulsions for wearable piezoresistive sensor and oil/water separation applications.
 J. Colloid Interface Sci. 618, 311–321. https://doi.org/10.1016/j.jcis.2022.03.073.
- Cao, H., Escamilla, M., Arole, K.D., Holta, D., Lutkenhaus, J.L., Radovic, M., Green, M.J., and Pentzer, E.B. (2021). Flocculation of MXenes and Their Use as 2D Particle Surfactants for Capsule Formation. Langmuir 37, 2649–2657. https://doi.org/10.1021/acs.langmuir.0c03244.
- Cao, H., Escamilla, M., Anas, M., Tan, Z., Gulati, S., Yun, J., Arole, K.D., Lutkenhaus, J.L., Radovic, M., Pentzer, E.B., and Green, M.J. (2021). Synthesis and Electronic Applications of Particle-Templated Ti3C2Tz MXene-Polymer Films via Pickering Emulsion Polymerization. ACS Appl. Mater. Interfaces 13, 51556–51566. https://doi.org/10.1021/acsami.1c16234.
- Klapper, M., Nenov, S., Haschick, R., Müller, K., and Müllen, K. (2008). Oil-in-Oil Emulsions: A Unique Tool for the Formation of Polymer Nanoparticles. Acc. Chem. Res. 41, 1190–1201. https://doi.org/10.1021/ar8001206.
- Rodier, B., de Leon, A., Hemmingsen, C., and Pentzer, E. (2017). Controlling Oil-in-Oil Pickering-Type Emulsions Using 2D Materials as Surfactant. ACS Macro Lett. 6, 1201–1206. https://doi.org/10.1021/acsmacrolett. 7b00648.

- Tan, J., Ruan, S., Zhang, M., He, H., Song, S., Yang, B., Nie, J., and Zhang, Q. (2022). Tailor-made urethane-linked alkyl-celluloses: a promising stabilizer for oil-in-oil Pickering emulsions. Polym. Chem. 13, 3144–3153. https://doi.org/10.1039/D2PY00431C.
- Zarour, A., Omar, S., and Abu-Reziq, R. (2021). Preparation of Poly(ethylene glycol)@Polyurea Microcapsules Using Oil/Oil Emulsions and Their Application as Microreactors. Polymers 13, 2566. https://doi.org/10.3390/ polym13152566.
- Müller, K., Klapper, M., and Müllen, K. (2007). Polyester nanoparticles by non-aqueous emulsion polycondensation. J. Polym. Sci. A. Polym. Chem. 45, 1101–1108. https://doi.org/ 10.1002/pola.21874.
- Zia, A., Pentzer, E., Thickett, S., and Kempe, K. (2020). Advances and Opportunities of Oil-in-Oil Emulsions. ACS Appl. Mater. Interfaces 12, 38845–38861. https://doi.org/10.1021/acsami. 0c0/7993.
- Rymaruk, M.J., Cunningham, V.J., Brown, S.L., Williams, C.N., and Armes, S.P. (2020). Oil-in-oil pickering emulsions stabilized by diblock copolymer nanoparticles. J. Colloid Interface Sci. 580, 354–364. https://doi.org/10.1016/j. jcis.2020.07.010.
- Müller, K., Klapper, M., and Müllen, K. (2007). Preparation of high molecular weight polyurethane particles by nonaqueous emulsion polyaddition. Colloid Polym. Sci. 285, 1157–1161. https://doi.org/10.1007/s00396-007-1670-4.
- Tyowua, A.T., Yiase, S.G., and Binks, B.P. (2017).
 Double oil-in-oil-in-oil emulsions stabilised solely by particles. J. Colloid Interface Sci. 488, 127–134. https://doi.org/10.1016/j.jcis.2016.10.089.
- Binks, B.P., and Tyowua, A.T. (2016). Oil-in-oil emulsions stabilised solely by solid particles. Soft Matter 12, 876–887. https://doi.org/10. 1039/C55M02438B.
- Lak, S.N., Ahmed, S., Shamberger, P.J., and Pentzer, E.B. (2022). Encapsulation of hygroscopic liquids via polymer precipitation in non-aqueous emulsions. J. Colloid Interface Sci. 628, 605–613. https://doi.org/10.1016/j. icis 2022 08 083
- Nahar, Y., Wei, P., Cipriani, C., Khodabandeh, A., Bissember, A.C., Pentzer, E.B., and Thickett, S.C. (2022). Open-Cell PolyHIPES from Polymerizable Eutectics: Tunable Morphology, Surface Modification, and Thermoresponsive Swelling Behavior. ACS Appl. Polym. Mater. 4, 8429– 8440. https://doi.org/10.1021/acsapm.2c01354.
- Lee, Y.-Y., Edgehouse, K., Klemm, A., Mao, H., Pentzer, E., and Gurkan, B. (2020). Capsules of Reactive Ionic Liquids for Selective Capture of Carbon Dioxide at Low Concentrations. ACS Appl. Mater. Interfaces 12, 19184–19193. https://doi.org/10.1021/acsami.0c01622.
- Rodier, B.J., de Leon, A., Hemmingsen, C., and Pentzer, E. (2018). Polymerizations in oil-in-oil emulsions using 2D nanoparticle surfactants. Polym. Chem. 9, 1547–1550. https://doi.org/ 10.1039/C7PY01819C.
- Wang, Y., Wei, P., Zhou, Q., Cipriani, C., Qi, M., Sukhishvili, S., and Pentzer, E. (2022).
 Temperature-Dependent Capsule Shell Bonding and Destruction Based on Hindered Poly(urea-urethane) Chemistry. Chem. Mater.

Please cite this article in press as: Cao et al., Structured $T_{i_3}C_2T_z$ MXene-polymer composites from non-aqueous emulsions, Matter (2024), https://doi.org/10.1016/j.matt.2024.02.011

Matter Article



- 34, 5821–5831. https://doi.org/10.1021/acs.chemmater.2c00415.
- Habib, T., Patil, N., Zhao, X., Prehn, E., Anas, M., Lutkenhaus, J.L., Radovic, M., and Green, M.J. (2019). Heating of Ti3C2Tx MXene/ polymer composites in response to Radio Frequency fields. Sci. Rep. 9, 16489. https://doi. org/10.1038/s41598-019-52972-2.
- 81. Zhao, X., Vashisth, A., Prehn, E., Sun, W., Shah, S.A., Habib, T., Chen, Y., Tan, Z., Lutkenhaus, J.L., Radovic, M., and Green, M.J. (2019). Antioxidants Unlock Shelf-Stable Ti3C2Tx
- (MXene) Nanosheet Dispersions. Matter 1, 513–526. https://doi.org/10.1016/j.matt.2019.05.020
- 82. Zhao, X., Cao, H., Coleman, B.J., Tan, Z., Echols, I.J., Pentzer, E.B., Lutkenhaus, J.L., Radovic, M., and Green, M.J. (2022). The Role of Antioxidant Structure in Mitigating Oxidation in Ti3C2Tx and Ti2CTx MXenes. Adv. Mater. Interfac. 9, 2200480. https://doi.org/10.1002/admi.202200480.
- 83. Athavale, S., Micci-Barreca, S., Arole, K., Kotasthane, V., Blivin, J., Cao, H.,
- Lutkenhaus, J.L., Radovic, M., and Green, M.J. (2023). Advances in the Chemical Stabilization of MXenes. Langmuir 39, 918–928. https://doi.org/10.1021/acs.langmuir.2c02051.
- 84. Zhao, X., Holta, D.E., Tan, Z., Oh, J.-H., Echols, I.J., Anas, M., Cao, H., Lutkenhaus, J.L., Radovic, M., and Green, M.J. (2020). Annealed Ti3C2Tz MXene Films for Oxidation-Resistant Functional Coatings. ACS Appl. Nano Mater. 3, 10578–10585. https://doi.org/10.1021/acsanm. 0c02473.